# Facile Synthesis of PdPt@Pt Nanorings Supported on Reduced Graphene Oxide with Enhanced Electrocatalytic Properties

Shan-Shan Li, Jing-Jing Lv, Li-Na Teng, Ai-Jun Wang,* Jian-Rong Chen, and Jiu-Ju Feng*

College of Chemistry and Life Science, College of Geography and Environmental Science, Zhejiang Normal University, Jinhua 321004, China

Ⓢ *Supporting Information*

ABSTRACT: In this work, a facile one-pot wet-chemical method was developed for the self-assembly of PdPt@Pt nanorings via in situ reduction of $[PdCl_4]^{2-}$ and $[PtCl_6]^{2-}$ at room temperature, which are simultaneously dispersed on reduced graphene oxide (rGO; denoted as PdPt@Pt/rGO). Hexadecylpyridinium chloride was demonstrated as a shape-directing agent and formic acid as a reducing agent during the reaction process. The as-prepared PdPt@Pt/rGO exhibited enhanced electrocatalytic activity and better stability for oxygen reduction reaction and ethanol oxidation reaction in acid media, compared with PtPd/rGO, Pt/rGO, Pd/rGO, Pt black, and Pt/C catalysts.
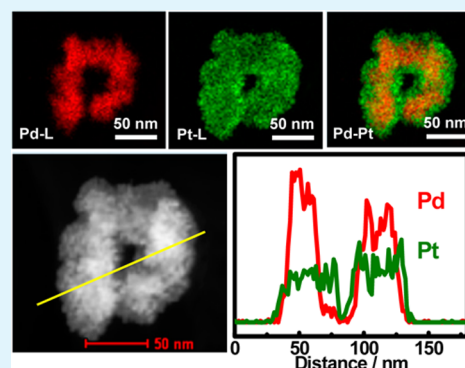
KEYWORDS: *reduced graphene oxide, nanorings, hexadecylpyridinium chloride, oxygen reduction reaction, ethanol oxidation reaction*

1. INTRODUCTION

Fuel cells have attracted considerable attention because they are promising candidates for providing clean energy.[1,2] Generally, a fuel cell is an electrochemical device that oxidizes fuel (e.g., hydrogen or alcohols) at the anode and reduces oxygen from air at the cathode to produce electricity.[1,2] The sluggish reduction kinetics of oxygen reduction reaction (ORR) at the cathode is one of the most critical challenges for commercial applications of fuel cells. Another important issue is the oxidation of hydrogen or alcohols (for example, methanol or ethanol) at the anode.[1] Among various liquid fuels, ethanol is particularly attractive because it is environmentally friendly and can be produced in a large scale from agricultural products that are easy to store and transport in comparison with hydrogen.[3,4] To our knowledge, platinum (Pt) and Pt-based nanomaterials are thought to be the most effective electrocatalysts for ORR and ethanol oxidation reaction (EOR). These materials seriously suffer from poor reaction kinetics and poisoning.[4−8] Therefore, the development of novel electrocatalysts with improved catalytic activity and durability is highly desirable but remains a significant challenge.

Bimetallic nanocrystals consisting of two distinct metals [e.g., Pt and palladium (Pd)] have broad applications in electrocatalytic reactions[3,9−13] owing to their combined properties associated with both metals, along with unexplored synergistic properties.[14,15] Among various metals around Pt in the periodic table, Pd is the best candidate to form bimetallic nanocrystals with Pt because Pt and Pd share the same face-centered-cubic (fcc) structure and almost identical lattice constants (with a mismatch of 0.77%).[9,16] Besides, Pd is less expensive than Pt,

and thereby the cost can be greatly reduced by using Pd as a base metal. Moreover, the introduction of Pd can effectively prevent the electrocatalysts from degradation in some degree. As a result, their stability is greatly improved by up-shifting the dissolution potential of Pt.[17] In addition, a combination of Pd and Pt may further enhance their catalytic performance and even extend their potential applications.

Recently, a number of synthetic methods have been developed for the preparation of Pd−Pt bimetallic nanocrystals with different structures, including cochemical reduction[6,18] and its combination with galvanic replacement[19] to produce alloy nanocrystals, galvanic replacement[20] between Pd nanocrystals and a Pt salt precursor to form dendritic nanostructures, seed-mediated overgrowth[21−23] to generate core−shell, multishell, and dendritic nanostructures, and a combination of electrodeposition and galvanic replacement[24] to deposit Pt monolayers on Pd nanocrystals. Among the aforementioned synthetic methods and structures, hollow structures are of great importance because of their excellent catalytic properties.

Graphene is an excellent two-dimensional support for dispersion of nanomaterials and maximization of the activity of the supported nanomaterials with different sizes, shapes, chemical compositions, and heterojunctions.[25] This is ascribed to its large specific surface area, excellent conductivity, and good stability.[25,26]
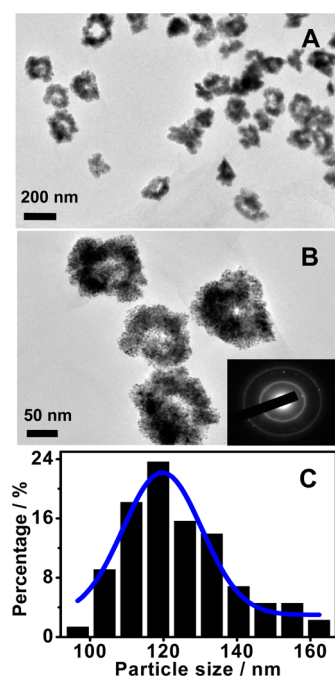
Self-assembly provides a very powerful strategy to prepare graphene/metal hybrids with high quality because many methods have been developed for the synthesis of high-quality metal nanoparticles with different sizes, components, and shapes.[27−29] For instance, Niu and co-workers fabricated hollow AuPd flowers self-assembled on ionic-liquid-functionalized graphene, showing good electrooxidation of formic acid.[30] In another case, Guo and Sun prepared monodispersed FePt nanoparticles assembled on graphene, showing enhanced catalytic activity and durability for ORR.[31]

Herein, a one-step wet-chemical method was developed for the direct self-assembly of PdPt@Pt nanorings on reduced graphene oxide (rGO) at room temperature, with the assistance of hexadecylpyridinium chloride (HDPC). The electrocatalytic properties of PdPt@Pt/rGO were investigated in some detail, using ORR and EOR as bench-model systems.
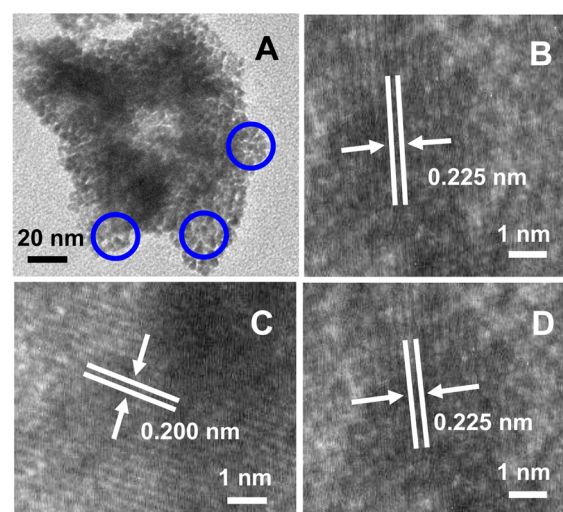
2. RESULTS AND DISCUSSION

2.1. Physical Characterization. Transmission electron microscopy (TEM) and high-resolution TEM (HR-TEM) were employed to characterize the morphology of the typical product. The product contains a lot of three-dimensional nanorings (Figures 1A,B and 2A), with a narrow size
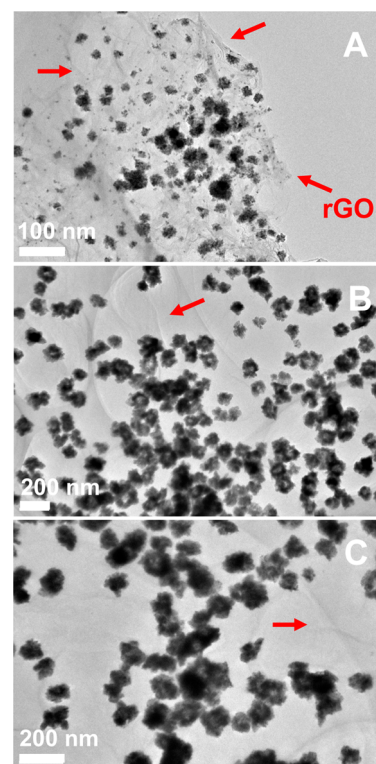

Figure 2. (A−D) HR-TEM images of PdPt@Pt/rGO.

kept the same (Figure 3A). Moreover, the structure is hardly obtained by using insufficient (Figure 3B) or excessive (Figure

Figure 1. (A and B) TEM images of PdPt@Pt/rGO. (C) The corresponding particle size distribution. The inset shows the corresponding SAED pattern.


Figure 3. Representative TEM images of PdPt@Pt/rGO obtained without (A) and with 1.25 mg (B) and 3.75 mg (C) of HDPC. Red arrows indicate the wrinkles of rGO.

distribution from 110 to 130 nm (Figure 1C), which are quite different from Pt/rGO (Figure S1A in the Supporting Information, SI) and Pd/rGO (Figure S1B in the SI). A careful survey of the TEM image reveals that each nanoring is actually a three-dimensionally interconnected porous nanostructure with primary Pd or Pt nanoparticles acting as building blocks. The mean diameter of the primary nanoparticles is about 4.5 nm (Figure 2A). Notably, PdPt@Pt nanorings are uniformly supported on the surfaces of rGO (i.e., using 2.50 mg of HDPC). However, the absence of HDPC yields irregular solid particles with serious aggregation, although other conditions are

3C) HDPC. These results manifest the critical role of HDPC and its amount in the formation of PdPt@Pt nanorings.

Moreover, the selective area electron diffraction (SAED) pattern (inset in Figure 1B) verifies the good crystallinity of PdPt@Pt nanorings. Figure 2A illustrates an individual PdPt@Pt nanoring with interplanar spacing of the lattice fringes of 0.225 and 0.200 nm, which correspond to the (111) and (200) lattice planes of fcc Pt (Figure 2B−D), respectively. Their chemical composition was determined by the energy-dispersive

10550

dx.doi.org/10.1021/am502148z | ACS Appl. Mater. Interfaces 2014, 6, 10549−10555

X-ray spectroscopy (EDS) analysis (Figure S2A in the SI), confirming the existence of carbon (C), Pt, and Pd elements. The atomic ratio of Pt to Pd is about 3:1. Additionally, the signal of copper (Cu) is observed in the EDS pattern, owing to the grid used for TEM measurements.

Furthermore, the distribution of each element in PdPt@Pt was examined by high-angle annular dark-field scanning transmission electron microscopy−energy-dispersive X-ray spectroscopy (HAADF-STEM−EDS) measurements (Figure 4). As measured by EDS elemental mapping (Figure 4A−C), Pt
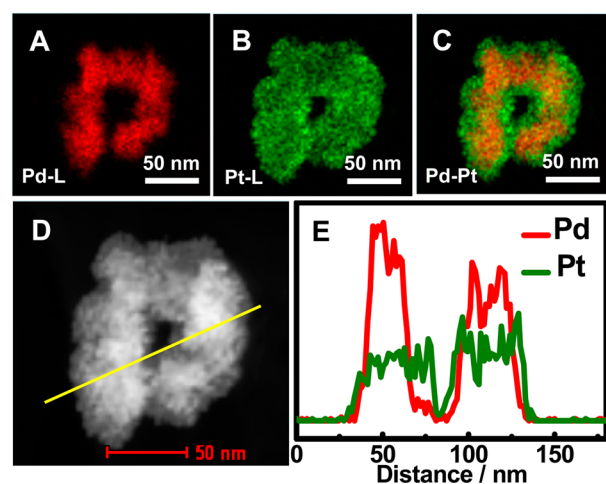

Figure 4. HAADF-STEM-EDS elemental mapping (A−C), HAADF-STEM image (D), and cross-sectional compositional line profiles (E) taken from a single PdPt@Pt nanoring.

is found throughout the whole nanoring, while Pd is only detected in the center region, showing the formation of a PdPt@Pt nanoring, as strongly manifested by the cross-sectional compositional line profiles (Figure 4D) with an even distribution of Pt and Pd. Meanwhile, the metal loading of PdPt@Pt nanorings on rGO is easily measured by thermogravimetric analysis (TGA) test, with a value of ca. 88 wt % (Figure S2B in the SI).

For the synthesis of PdPt@Pt nanorings supported on rGO, a one-step strategy was involved through a wet-chemical method with the help of HDPC. In the reaction system, HDPC as a cationic surfactant can form spherical micelles, in which the hydrophobic hydrocarbon chains point to the interior and the hydrophilic cationic groups point to the exterior. As a result, $[PdCl_4]^{2-}$ and $[PtCl_6]^{2-}$ are mainly located on the surface of the spherical micelles because of the electrostatic attraction. The formation mechanism of PdPt@Pt/rGO can be described as follows. First, HDPC and $[PdCl_4]^{2-}$ (and/or $[PtCl_6]^{2-}$) would be sequentially connected from inside to outside, owing to the electrostatic interactions. Second, the spherical micelles further form an adsorbed monolayer on the surface of rGO by intermolecular interactions. After the introduction of formic acid, the adsorbed $[PdCl_4]^{2-}$ and $[PtCl_6]^{2-}$ would be in situ reduced accordingly. In the present system, $[PdCl_4]^{2-}$ is more easily reduced than $[PtCl_6]^{2-}$, although the standard reduction potential of $[PtCl_6]^{2-}$ (0.740 V vs SHE) is more negative than that of $[PdCl_4]^{2-}$ (0.915 V vs SHE) under the same conditions. Therefore, the reduction of $[PdCl_4]^{2-}$ preferentially occurs at the very early stage, which serves as an in situ seed for the subsequent deposition of Pt. Using formic acid as a reducing agent, different reduction kinetics of $[PdCl_4]^{2-}$ and $[PtCl_6]^{2-}$

causes spontaneous separation between interior Pd and exterior Pt. Finally, PdPt@Pt/rGO was obtained by the careful removal of HDPC with water and ethanol.

Figure 5 shows the X-ray diffraction (XRD) patterns of PdPt@Pt/rGO (curve a), rGO (curve b), and GO (curve c).
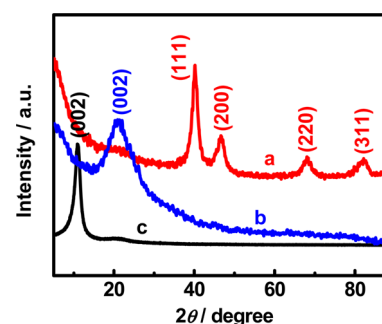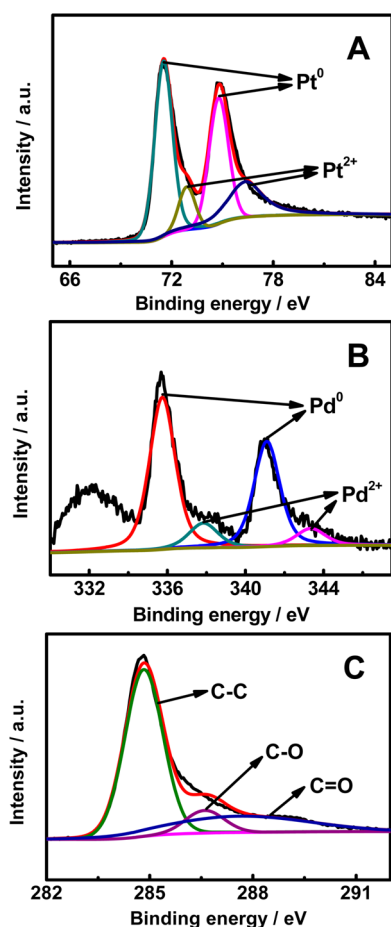

Figure 5. XRD patterns of PdPt@Pt/rGO (curve a), rGO (curve b), and GO (curve c).

For PdPt@Pt/rGO (curve a), the four representative diffraction peaks at 40.2°, 46.6°, 68.1°, and 82.2° are attributed to the (111), (200), (220), and (311) planes of fcc Pt and Pd, respectively. Besides, the average diameter of Pt or Pd nanoparticles is about 4.7 nm calculated from the Scherrer equation from the XRD pattern of PdPt@Pt/rGO (curve a). It should be pointed out that the average particle size is a little larger, compared with that obtained from the TEM image. It is likely that oriented attachment of primary Pd or Pt crystallites in the hierarchical nanorings is responsible for the big particle size calculated from the XRD data.[32] These results demonstrate that the nanorings are composed of Pt and Pd bimetals rather than their alloy,[33,34] as supported by the HAADF-STEM-EDS analysis. This is due to the different reduction potentials of $[PdCl_4]^{2-}$ and $[PtCl_6]^{2-}$ in the present work. Additionally, a broad diffraction peak at 23.0° is detected for PdPt@Pt/rGO (curve a) and rGO (curve b), while it is different from GO only with a strong peak at 11.0° corresponding to the (002) planes of GO (curve c), revealing efficient reduction of GO to rGO.

X-ray photoelectron spectrometry (XPS) measurements were performed to analyze the composition and surface oxidation states of a catalyst. Figure 6 shows the high-resolution Pt 4f, Pd 3d, and C 1s XPS spectra of PdPt@Pt/rGO. According to their elemental components, the molar ratio of Pt to Pd is estimated to be 3:1, which is consistent with the EDS data.

As to the spectrum of Pt 4f (Figure 6A), two main peaks located at 71.5 and 74.7 eV correspond to metallic Pt, whereas the other two minor peaks at 72.9 and 76.4 eV are attributed to platinum oxide such as $Pt(OH)_2$ and/or PtO.[35] Similarly, the splitting pattern of Pd 3d consists of two doublets (Figure 6B): the strong doublet (335.7 and 341.0 eV) is due to metallic Pd, and the other doublet (337.8 and 343.3 eV) belongs to Pd^{2+}.[8,36] Therefore, compared with Pt/rGO (Figure S3A in the SI) and Pd/rGO (Figure S3B in the SI), the peaks of Pt^0 and Pd^0 for PdPt@Pt/rGO both show a positive shift, further reflecting a strong interactions between Pt and Pd.[37,38]

Obviously, metallic Pt and Pd are the main species in PdPt@Pt/rGO. Therefore, it is expected to be an effective electrocatalyst for ORR and EOR. The existence of Pt^{2+} and Pd^{2+} can be ascribed to the incomplete reduction of $[PtCl_6]^{2-}$ and $[PdCl_4]^{2-}$ by formic acid via the wet-chemical method,

Figure 6. High-resolution XPS spectra of Pt 4f (A), Pd 3d (B), and C 1s (C) for PdPt@Pt/rGO.

rGO (curve b), and 0.99 for GO (curve c), indicating the decreased size of the sp^2 domains and partially ordered crystal structures of rGO.[49,50] Therefore, the formation of rGO is attributed to the good electrical conductivity of PdPt@Pt/rGO.

2.2. Electrocatalytic Reduction of Oxygen. Cyclic voltammetry (CV) curves were recorded for a preliminary study of the electrochemical properties of PdPt@Pt/rGO modified electrodes, using PtPd/rGO, Pt/rGO, Pd/rGO, Pt black, and 10% Pt/C catalysts as references (Figure 7A).
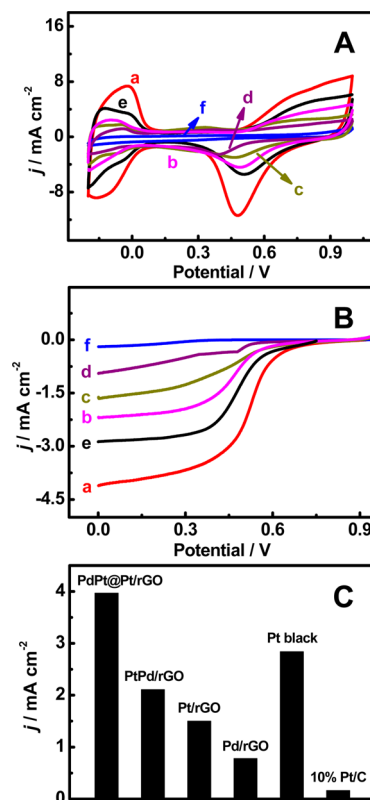
Figure 7. (A) CV curves of PdPt@Pt/rGO (curve a), PtPd/rGO (curve b), Pt/rGO (curve c), Pd/rGO (curve d), Pt black (curve e), and 10% Pt/C (curve f) catalyst-modified electrodes in 0.5 M H$_2$SO$_4$ at a scan rate of 50 mV s^{-1}. (B) ORR polarization curves of PdPt@Pt/rGO (curve a), PtPd/rGO (curve b), Pt/rGO (curve c), Pd/rGO (curve d), Pt black (curve e), and 10% Pt/C (curve f) catalyst-modified electrodes in O$_2$-saturated 0.5 M H$_2$SO$_4$ at a scan rate of 5 mV s^{-1}, using a rotation rate of 1600 rpm. (C) Corresponding specific current density at 0.1 V.

along with the easy oxidation of the surface Pt and Pd to form platinum and palladium oxide under ambient conditions.[39,40]

Figures 6C and S3C in the SI show C 1s spectra of PdPt@Pt/rGO and GO that are deconvoluted into three main peaks: the alkyl C and sp^2-bonded C network (C−C/C=C), the C−O of the hydroxyl and epoxyl groups, and the carbonyl C (C=O).[41] The intensity ratio of the C−C to C−O bands is much larger for PdPt@Pt/rGO in comparison with that of GO, indicating efficient reduction of GO to rGO in the present work.

Effective reduction of GO is further confirmed by Fourier transform infrared (FT-IR) spectra (Figure S4A in the SI). There are two peaks at 1627 and 3434 cm^{-1} in each sample, which are assigned to the C=C skeletal vibration of the sp^2-hybridized C atoms[42] and the O−H stretching vibration of the C−OH groups and water,[43,44] respectively. The absorption peak at 1062 cm^{-1} is clearly observed for GO (curve c), corresponding to the C−O stretching vibration of the epoxy C−O group.[36,45] However, this peak is hardly detected for PdPt@Pt/rGO (curve a) and rGO (curve b).

Raman spectroscopy is another powerful tool to evaluate the structural defects, number of layers, and doping level of graphene.[46−48] For PdPt@Pt/rGO (Figure S4B in the SI, curve a), there are two strong characteristic peaks at 1352 cm^{-1} for the D band and 1595 cm^{-1} for the G band. The two bands display a slight blue shift in comparison with GO (Figure S4B in the SI, curve c). Meanwhile, the intensity ratios of the D to G bands (I_D/I_G) are 2.00 for PdPt@Pt/rGO (curve a), 1.85 for

Clearly, all of the CV curves exhibit three traditional distinctive potential regions associated with hydrogen adsorption/desorption processes in the potential range of −0.20 to 0.10 V, the double layer located from 0.10 to 0.40 V, and the formation/reduction of the surface oxide that emerged above 0.40 V.[51,52] The electrochemically active surface area (EASA) of PdPt@Pt/rGO (58.9 m^2 g^{-1}) is higher than that of PtPd/rGO (20.5 m^2 g^{-1}), Pt/rGO (17.0 m^2 g^{-1}), Pd/rGO (14.0 m^2 g^{-1}), Pt black (29.6 m^2 g^{-1}), and 10% Pt/C (10.8 m^2 g^{-1}) catalysts, owing to serious agglomeration in Pt black and 10% Pt/C (Figure S5A,B in the SI). The porous nanoring-like structure of PdPt@Pt/rGO provides a reasonably enlarged surface area despite its relatively large overall particle size.

Figure 7B shows the corresponding ORR polarization curves. For PdPt@Pt/rGO modified electrodes, the diffusion-limited currents were obtained in the potential region below 0.30 V,

whereas the mixed kinetics—diffusion control region occurs between 0.30 and 0.75 V. As illustrated in Figure 7C, the diffusion-limited current density of PdPt@Pt/rGO is much higher than that of the other catalysts. The onset potential (0.75 V) and half-wave potential (0.55 V) of PdPt@Pt/rGO are more positive, compared with the other cases. These results suggest that PdPt@Pt/rGO is superior to PtPd/rGO, Pt/rGO, Pd/rGO, Pt black, and 10% Pt/C catalysts under the same conditions.

Figure 8A shows a series of polarization curves toward ORR on a PdPt@Pt/rGO modified electrode in O_2-saturated 0.5 M
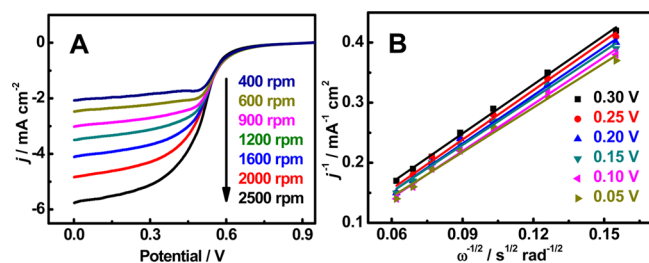
Figure 8. (A) ORR polarization curves of PdPt@Pt/rGO obtained in 0.5 M H_2SO_4 at a scan rate of 5 mV s^{-1} with different rotation rates. (B) Associated Koutecky−Levich plots obtained at different potentials.

H_2SO_4 at a scan rate of 5 mV s^{-1}. The onset potential is 0.75 V, and the reduction currents sharply increase to their diffusion-limited current densities. The corresponding Koutecky−Levich plots (Figure 8B) at different potentials and the number of electrons involved per O_2 molecule reduction can be determined using the Koutecky−Levich equation. The electron-transfer number (n) is calculated as 3.9−4.1, revealing that ORR is dominated by a four-electron pathway where O_2 is directly reduced to H_2O.

2.3. Electrocatalytic Oxidation of Ethanol. To further investigate the electrocatalytic performance of the as-prepared catalyst, EOR was investigated on PdPt@Pt/rGO, PtPd/rGO, Pt/rGO, Pd/rGO, Pt black, and 10% Pt/C catalyst-modified electrodes. Figure S6A in the SI shows the corresponding CV curves in 0.5 M H_2SO_4 containing 0.5 M ethanol at a scan rate of 50 mV s^{-1}. In all of the CV curves, two anodic peaks were observed in the positive scan and the reversed negative scan, which are well-known to reflect the electrooxidation of ethanol and intermediate carbonaceous species (e.g., CO), respectively. Through a comparison of the CV curves, PdPt@Pt/rGO displays better electrochemical activity compared with the other catalysts, judging from the highest peak current density and the negative onset potential for EOR. As shown in Figure S6A in the SI, the peak current density is 74.2 mA mg^{-1} for PdPt@Pt/rGO, which is approximately 2.0, 2.8, 5.4, 1.3, and 9.4 times higher than those of PtPd/rGO (37.6 mA mg^{-1}), Pt/rGO (26.7 mA mg^{-1}), Pd/rGO (13.7 mA mg^{-1}), Pt black (57.8 mA mg^{-1}), and 10% Pt/C (7.9 mA mg^{-1}) catalysts, respectively. It indicates that PdPt@Pt/rGO has a large number of active sites available for EOR, which agrees well with the above results of EASA.

Furthermore, in order to estimate the tolerance of the catalysts, chronoamperometric measurements were performed in 0.5 M H_2SO_4 containing 0.5 M ethanol. Figure S6B in the SI shows the current−time curves for EOR measured at a fixed potential of 0.6 V on PdPt@Pt/rGO modified electrodes, using PtPd/rGO, Pt/rGO, Pd/rGO, Pt black, and 10% Pt/C catalysts as references. The polarization currents showed a rapid decay

during the initial period because of poisoning of the intermediate species (e.g., CO). A higher initial current and a much slower current decay are detected for PdPt@Pt/rGO, compared with those of PtPd/rGO, Pt/rGO, Pd/rGO, Pt black, and 10% Pt/C catalysts. At the end of the test, the oxidation current was still considerably higher for PdPt@Pt/rGO than the other catalysts, further confirming relatively better tolerance of the intermediate species and higher catalytic activity of PdPt@Pt/rGO. Meanwhile, a slightly negative CO stripping potential is observed for PdPt@Pt/rGO, compared with Pt black and 10% Pt/C catalysts, revealing that PdPt@Pt/rGO facilitates the oxidation of CO (Figure S7 in the SI).

Accelerated CV measurement was carried out to evaluate the catalytic stability of PdPt@Pt/rGO modified electrodes. The corresponding 20th, 300th, 600th, and 1000th CV curves were provided (Figure 9A), and the corresponding EASA changes
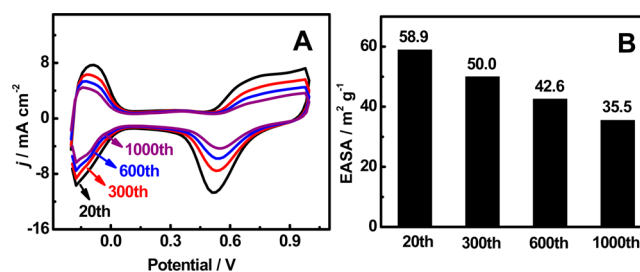
Figure 9. (A) CV curves of PdPt@Pt/rGO before and after an accelerated durability test. (B) EASA of PdPt@Pt/rGO at the corresponding cycle number.

were also presented (Figure 9B) for comparison. Clearly, using the EASA of the 20th cycle as a reference, the EASA displays a loss of 15%, 27%, and 40% in EASA after 300, 600, and 1000 cycles, respectively. These results further verify the enhanced durability of PdPt@Pt/rGO, which is in good agreement with the chronoamperometric measurements.

PdPt@Pt/rGO exhibits enhanced catalytic activity and good stability for ORR and EOR. The superior electrocatalytic performances can be attributed to a small mismatch in the lattice constants between Pt and Pd,[9] the changes in the d-band properties of Pt caused by coupling with Pd,[9,53] Pd as a promoter for the oxidative removal of CO on the Pt surface by available oxygen-containing species formed on neighboring secondary metal particles,[54] high loading and well-dispersed PdPt@Pt nanorings on rGO, and good electrical conductivity of graphene.

3. CONCLUSIONS

In summary, we have reported a simple and general strategy for the synthesis of PdPt@Pt/rGO with the assistance of HDPC at room temperature, without using any toxic organic solvent, seed, or template. Significantly, the as-prepared bimetallic nanocomposites exhibited enhanced electrocatalytic activity and better stability for ORR and EOR in acid media. Because of facile preparation and improved electrocatalytic performances, the as-synthesized PdPt@Pt/rGO may find promising potential applications in fuel cells, electrochemical sensor, and hydrogen gas sensing.

■ ASSOCIATED CONTENT

⑤ Supporting Information

Experimental sections, TEM images, EDS pattern, XPS, FT-IR, and Raman spectra, TGA, CV, and chronoamperometric curves, as well as CO-stripping voltammograms. This material is available free of charge via the Internet at http://pubs.acs.org.

■ AUTHOR INFORMATION

Corresponding Authors

*E-mail: ajwang@zjnu.cn.
*E-mail: jjfeng@zjnu.cn.

Notes

The authors declare no competing financial interest.

■ ACKNOWLEDGMENTS

■ REFERENCES

(1) Debe, M. K. Electrocatalyst Approaches and Challenges for Automotive Fuel Cells. *Nature* **2012**, *486*, 43−51.

(2) Mazumder, V.; Lee, Y.; Sun, S. Recent Development of Active Nanoparticle Catalysts for Fuel Cell Reactions. *Adv. Funct. Mater.* **2010**, *20*, 1224−1231.

(3) Zhu, C.; Guo, S.; Dong, S. PdM (M = Pt, Au) Bimetallic Alloy Nanowires with Enhanced Electrocatalytic Activity for Electro-Oxidation of Small Molecules. *Adv. Mater.* **2012**, *24*, 2326−2331.

(4) Koenigsmann, C.; Wong, S. S. One-Dimensional Noble Metal Electrocatalysts: A Promising Structural Paradigm for Direct Methanol Fuel Cells. *Energy Environ. Sci.* **2011**, *4*, 1161−1176.

(5) Ruan, L.; Zhu, E.; Chen, Y.; Lin, Z.; Huang, X.; Duan, X.; Huang, Y. Biomimetic Synthesis of an Ultrathin Platinum Nanowire Network with a High Twin Density for Enhanced Electrocatalytic Activity and Durability. *Angew. Chem., Int. Ed.* **2013**, *52*, 12577−12581.

(6) Yin, A.-X.; Min, X.-Q.; Zhang, Y.-W.; Yan, C.-H. Shape-Selective Synthesis and Facet-Dependent Enhanced Electrocatalytic Activity and Durability of Monodisperse Sub-10 nm Pt−Pd Tetrahedrons and Cubes. *J. Am. Chem. Soc.* **2011**, *133*, 3816−3819.

(7) Lv, J.-J.; Li, S.-S.; Zheng, J.-N.; Wang, A.-J.; Chen, J.-R.; Feng, J.-J. Facile Synthesis of Reduced Graphene Oxide Supported PtAg Nanoflowers and Their Enhanced Electrocatalytic Activity. *Int. J. Hydrogen Energy* **2014**, *39*, 3211−3218.

(8) Fu, G.; Wu, K.; Lin, J.; Tang, Y.; Chen, Y.; Zhou, Y.; Lu, T. One-Pot Water-Based Synthesis of Pt−Pd Alloy Nanoflowers and Their Superior Electrocatalytic Activity for the Oxygen Reduction Reaction and Remarkable Methanol-Tolerant Ability in Acid Media. *J. Phys. Chem. C* **2013**, *117*, 9826−9834.

(9) Zhang, H.; Jin, M.; Xia, Y. Enhancing the Catalytic and Electrocatalytic Properties of Pt-Based Catalysts by Forming Bimetallic Nanocrystals with Pd. *Chem. Soc. Rev.* **2012**, *41*, 8035−8049.

(10) Wang, M.; Zhang, W.; Wang, J.; Wexler, D.; Poynton, S. D.; Slade, R. C. T.; Liu, H.; Winther-Jensen, B.; Kerr, R.; Shi, D.; Chen, J. PdNi Hollow Nanoparticles for Improved Electrocatalytic Oxygen Reduction in Alkaline Environments. *ACS Appl. Mater. Interfaces* **2013**, *5*, 12708−12715.

(11) Zhang, H.; Xu, X.; Gu, P.; Li, C.; Wu, P.; Cai, C. Microwave-Assisted Synthesis of Graphene-Supported Pd₁Pt₃ Nanostructures and Their Electrocatalytic Activity for Methanol Oxidation. *Electrochim. Acta* **2011**, *56*, 7064−7070.

(12) Zhang, H.; Yin, Y.; Hu, Y.; Li, C.; Wu, P.; Wei, S.; Cai, C. Pd@Pt Core−Shell Nanostructures with Controllable Composition Synthesized by a Microwave Method and Their Enhanced Electrocatalytic Activity toward Oxygen Reduction and Methanol Oxidation. *J. Phys. Chem. C* **2010**, *114*, 11861−11867.

(13) Zheng, J.-N.; Li, S.-S.; Ma, X.; Chen, F.-Y.; Wang, A.-J.; Chen, J.-R.; Feng, J.-J. Green Synthesis of Core−Shell Gold−Palladium@Palladium Nanocrystals Dispersed on Graphene with Enhanced Catalytic Activity toward Oxygen Reduction and Methanol Oxidation in Alkaline Media. *J. Power Sources* **2014**, *262*, 270−278.

(14) Yang, H. Platinum-Based Electrocatalysts with Core−Shell Nanostructures. *Angew. Chem., Int. Ed.* **2011**, *50*, 2674−2676.

(15) Habas, S. E.; Lee, H.; Radmilovic, V.; Somorjai, G. A.; Yang, P. Shaping Binary Metal Nanocrystals through Epitaxial Seeded Growth. *Nat. Mater.* **2007**, *6*, 692−697.

(16) Wang, L.; Yamauchi, Y. Metallic nanocages: Synthesis of Bimetallic Pt−Pd Hollow Nanoparticles with Dendritic Shells by Selective Chemical Etching. *J. Am. Chem. Soc.* **2013**, *135*, 16762−16765.

(17) Ramirez-Caballero, G. E.; Hirunsit, P.; Balbuena, P. B. Shell−Anchor−Core Structures for Enhanced Stability and Catalytic Oxygen Reduction Activity. *J. Chem. Phys.* **2010**, *133*, 1−8.

(18) Liu, Y.; Chi, M.; Mazumder, V.; More, K. L.; Soled, S.; Henao, J. D.; Sun, S. Composition-Controlled Synthesis of Bimetallic PdPt Nanoparticles and Their Electro-Oxidation of Methanol. *Chem. Mater.* **2011**, *23*, 4199−4203.

(19) Zhang, H.; Jin, M.; Liu, H.; Wang, J.; Kim, M. J.; Yang, D.; Xie, Z.; Liu, J.; Xia, Y. Facile Synthesis of Pd−Pt Alloy Nanocages and Their Enhanced Performance for Preferential Oxidation of CO in Excess Hydrogen. *ACS Nano* **2011**, *5*, 8212−8222.

(20) Zhang, H.; Jin, M.; Wang, J.; Li, W.; Camargo, P. H. C.; Kim, M. J.; Yang, D.; Xie, Z.; Xia, Y. Synthesis of Pd−Pt Bimetallic Nanocrystals with a Concave Structure through a Bromide-Induced Galvanic Replacement Reaction. *J. Am. Chem. Soc.* **2011**, *133*, 6078−6089.

(21) Lim, B.; Jiang, M.; Camargo, P. H. C.; Cho, E. C.; Tao, J.; Lu, X.; Zhu, Y.; Xia, Y. Pd−Pt Bimetallic Nanodendrites with High Activity for Oxygen Reduction. *Science* **2009**, *324*, 1302−1305.

(22) Zhang, H.; Jin, M.; Wang, J.; Kim, M. J.; Yang, D.; Xia, Y. Nanocrystals Composed of Alternating Shells of Pd and Pt Can Be obtained by Sequentially Adding Different Precursors. *J. Am. Chem. Soc.* **2011**, *133*, 10422−10425.

(23) Peng, Z.; Yang, H. Synthesis and Oxygen Reduction Electrocatalytic Property of Pt-on-Pd Bimetallic Heteronanostructures. *J. Am. Chem. Soc.* **2009**, *131*, 7542−7543.

(24) Sasaki, K.; Naohara, H.; Cai, Y.; Choi, Y. M.; Liu, P.; Vukmirovic, M. B.; Wang, J. X.; Adzic, R. R. Core-Protected Platinum Monolayer Shell High-Stability Electrocatalysts for Fuel-Cell Cathodes. *Angew. Chem., Int. Ed.* **2010**, *49*, 8602−8607.

(25) Guo, S.; Dong, S. Graphene Nanosheet: Synthesis, Molecular Engineering, Thin Film, Hybrids, and Energy and Analytical Applications. *Chem. Soc. Rev.* **2011**, *40*, 2644−2672.

(26) Huang, X.; Qi, X.; Boey, F.; Zhang, H. Graphene-Based Composites. *Chem. Soc. Rev.* **2012**, *41*, 666−686.

(27) Liu, J.; Fu, S.; Yuan, B.; Li, Y.; Deng, Z. Toward a Universal "Adhesive Nanosheet" for the Assembly of Multiple Nanoparticles Based on a Protein-Induced Reduction/Decoration of Graphene Oxide. *J. Am. Chem. Soc.* **2010**, *132*, 7279−7281.

(28) Hong, W.; Bai, H.; Xu, Y.; Yao, Z.; Gu, Z.; Shi, G. Preparation of Gold Nanoparticle/Graphene Composites with Controlled Weight Contents and Their Application in Biosensors. *J. Phys. Chem. C* **2010**, *114*, 1822−1826.

(29) Liu, J.; Li, Y.; Li, Y.; Li, J.; Deng, Z. Noncovalent DNA Decorations of Graphene Oxide and Reduced Graphene Oxide toward Water-Soluble Metal−Carbon Hybrid Nanostructures via Self-Assembly. *J. Mater. Chem.* **2010**, *20*, 900−906.

(30) Chai, J.; Li, F.; Hu, Y.; Zhang, Q.; Han, D.; Niu, L. Hollow Flower-Like AuPd Alloy Nanoparticles: One Step Synthesis, Self-Assembly on Ionic Liquid-Functionalized Graphene, and Electro-oxidation of Formic Acid. *J. Mater. Chem.* **2011**, *21*, 17922−17929.

(31) Guo, S.; Sun, S. FePt Nanoparticles Assembled on Graphene as Enhanced Catalyst for Oxygen Reduction Reaction. *J. Am. Chem. Soc.* **2012**, *134*, 2492−2495.

(32) Zhang, L.; Zhang, J.; Jiang, Z.; Xie, S.; Jin, M.; Han, X.; Kuang, Q.; Xie, Z.; Zheng, L. Facile Syntheses and Electrocatalytic Properties of Porous Pd and its Alloy Nanospheres. *J. Mater. Chem.* **2011**, *21*, 9620−9625.

(33) Chu, Y. Y.; Wang, Z. B.; Cao, J.; Gu, D. M.; Yin, G. P. Ultrahigh Durable PtPd/C Nanowire Networks Catalyst Synthesized by Modified Phase Transfer Method for Methanol Oxidation. *Fuel Cells* **2013**, *13*, 380−386.

(34) Li, S.-S.; Zheng, J.-N.; Ma, X.; Hu, Y.-Y.; Wang, A.-J.; Chen, J.-R.; Feng, J.-J. Facile Synthesis of Hierarchical Dendritic PtPd Nanogarlands Supported on Reduced Graphene Oxide with Enhanced Electrocatalytic Properties. *Nanoscale* **2014**, *6*, 5708−5713.

(35) Chetty, R.; Kundu, S.; Xia, W.; Bron, M.; Schuhmann, W.; Chirila, V.; Brandl, W.; Reinecke, T.; Muhler, M. PtRu Nanoparticles Supported on Nitrogen-Doped Multiwalled Carbon Nanotubes as Catalyst for Methanol Electrooxidation. *Electrochim. Acta* **2009**, *54*, 4208−4215.

(36) Wang, Y.; Liu, H.; Wang, L.; Wang, H.; Du, X.; Wang, F.; Qi, T.; Lee, J.-M.; Wang, X. Pd catalyst Supported on a Chitosan-Functionalized Large-Area 3D Reduced Graphene Oxide for Formic Acid Electrooxidation Reaction. *J. Mater. Chem.* **2013**, *1*, 6839−6848.

(37) Cui, Z.; Feng, L.; Liu, C.; Xing, W. Pt Nanoparticles Supported on WO_3/C Hybrid Materials and Their Electrocatalytic Activity for Methanol Electro-Oxidation. *J. Power Sources* **2011**, *196*, 2621−2626.

(38) Sharma, C. S.; Awasthi, R.; Singh, R. N.; Sinha, A. S. K. Graphene−Cobaltite−Pd Hybrid Materials for Use as Efficient Bifunctional Electrocatalysts in Alkaline Direct Methanol Fuel Cells. *Phys. Chem. Chem. Phys.* **2013**, *15*, 20333−20344.

(39) Ohashi, M.; Beard, K. D.; Ma, S.; Blom, D. A.; St-Pierre, J.; Van Zee, J. W.; Monnier, J. R. Electrochemical and Structural Characterization of Carbon-Supported Pt−Pd Bimetallic Electrocatalysts Prepared by Electroless Deposition. *Electrochim. Acta* **2010**, *55*, 7376−7384.

(40) Feng, L.; Si, F.; Yao, S.; Cai, W.; Xing, W.; Liu, C. Effect of Deposition Sequences on Electrocatalytic Properties of PtPd/C Catalysts for Formic Acid Electrooxidation. *Catal. Commun.* **2011**, *12*, 772−775.

(41) Li, F.; Guo, Y.; Chen, M.; Qiu, H.; Sun, X.; Wang, W.; Liu, Y.; Gao, J. Comparison Study of Electrocatalytic Activity of Reduced Graphene Oxide Supported Pt−Cu Bimetallic or Pt Nanoparticles for the Electrooxidation of Methanol and Ethanol. *Int. J. Hydrogen Energy* **2013**, *38*, 14242−14249.

(42) Yue, W.; Lin, Z.; Jiang, S.; Yang, X. Preparation of Graphene-Encapsulated Mesoporous Metal Oxides and Their Application as Anode Materials for Lithium-Ion Batteries. *J. Mater. Chem.* **2012**, *22*, 16318−16323.

(43) Li, S.-S.; Lv, J.-J.; Hu, Y.-Y.; Zheng, J.-N.; Chen, J.-R.; Wang, A.-J.; Feng, J.-J. Facile Synthesis of Porous Pt−Pd Nanospheres Supported on Reduced Graphene Oxide Nanosheets for Enhanced Methanol Electrooxidation. *J. Power Sources* **2014**, *247*, 213−218.

(44) Li, S.-S.; Hu, Y.-Y.; Feng, J.-J.; Lv, Z.-Y.; Chen, J.-R.; Wang, A.-J. Rapid Room-Temperature Synthesis of Pd Nanodendrites on Reduced Graphene Oxide for Catalytic Oxidation of Ethylene Glycol and Glycerol. *Int. J. Hydrogen Energy* **2014**, *39*, 3730−3738.

(45) Gao, L.; Yue, W.; Tao, S.; Fan, L. Novel Strategy for Preparation of Graphene−Pd, Pt Composite, and Its Enhanced Electrocatalytic Activity for Alcohol Oxidation. *Langmuir* **2012**, *29*, 957−964.

(46) Hu, T.; Zhou, J.; Dong, J. Vibrational Properties and Raman Spectra of Different Edge Graphene Nanoribbons, Studied by First-Principles Calculations. *Phys. Lett. A* **2013**, *377*, 399−404.

(47) Cuong, T. V.; Pham, V. H.; Tran, Q. T.; Hahn, S. H.; Chung, J. S.; Shin, E. W.; Kim, E. J. Photoluminescence and Raman Studies of Graphene Thin Films Prepared by Reduction of Graphene Oxide. *Mater. Lett.* **2010**, *64*, 399−401.

(48) Ferrari, A. C. Raman Spectroscopy of Graphene and Graphite: Disorder, Electron-Phonon Coupling, Doping and Nonadiabatic Effects. *Solid State Commun.* **2007**, *143*, 47−57.

(49) Wang, H.; Maiyalagan, T.; Wang, X. Review on Recent Progress in Nitrogen-Doped Graphene: Synthesis, Characterization, and Its Potential Applications. *ACS Catal.* **2012**, *2*, 781−794.

(50) An, X.; Liu, F.; Jung, Y. J.; Kar, S. Large-Area Synthesis of Graphene on Palladium and Their Raman Spectroscopy. *J. Phys. Chem. C* **2012**, *116*, 16412−16420.

(51) Lu, Y.; Jiang, Y.; Wu, H.; Chen, W. Nano-PtPd Cubes on Graphene Exhibit Enhanced Activity and Durability in Methanol Electrooxidation after CO Stripping-Cleaning. *J. Phys. Chem. C* **2013**, *117*, 2926−2938.

(52) He, W.; Jiang, H.; Zhou, Y.; Yang, S.; Xue, X.; Zou, Z.; Zhang, X.; Akins, D. L.; Yang, H. An Efficient Reduction Route for the Production of Pd−Pt Nanoparticles Anchored on Graphene Nanosheets for Use as Durable Oxygen Reduction Electrocatalysts. *Carbon* **2012**, *50*, 265−274.

(53) Wakisaka, M.; Mitsui, S.; Hirose, Y.; Kawashima, K.; Uchida, H.; Watanabe, M. Electronic Structures of Pt−Co and Pt−Ru Alloys for CO-Tolerant Anode Catalysts in Polymer Electrolyte Fuel Cells Studied by EC−XPS. *J. Phys. Chem. B* **2006**, *110*, 23489−23496.

(54) Wang, H.; Xu, C.; Cheng, F.; Zhang, M.; Wang, S.; Jiang, S. P. Pd/Pt Core−Shell Nanowire Arrays as Highly Effective Electrocatalysts for Methanol Electrooxidation in Direct Methanol Fuel Cells. *Electrochem. Commun.* **2008**, *10*, 1575−1578.